

Títol del treball:

Modifying catalytic sustainability: aromaticity, conceptual DFT and steric mapping

Nom estudiant: Carles Alcaide i Blaya

Correu electrònic: carlesalcaideblaya@gmail.com

Grau en: Química

Nom del tutor: Dr. Albert Poater Teixidor

Correu electrònic: albert.poater@udg.edu

Nom de la tutora: Dra. Sílvia Simon Rabaseda

Correu electrònic: silvia.simon@udg.edu

Contents

Resum	i
Resumen	ii
Abstract	iii
Ethics, sustainability and gender perspective reflections	iv
1 Introduction	1
2 Objectives	5
3 Methodology	6
3.1 Electronic and geometrical indices	6
3.1.1 Atomic charges	6
3.1.2 Mayer Bond Order (MBO)	6
3.1.3 Fukui function	7
3.2 Steric maps	7
3.3 Aromaticity	8
4 Results and discussion	10
4.1 Scope of catalysts by predictive chemistry	10
4.2 Kinetic cost	12
4.3 Structural characterisation	13
4.4 Steric maps	16
4.5 Aromaticity	18
5 Conclusions	23
References	26
A Appendix	27
A.1 Steric maps for intermediate III	27
A.2 Tables of aromaticity indices for the others intermediates	28

Resum

La hidrogenació catalítica és un procés crucial en les indústries químiques i farmacèutiques. Els catalitzadors tradicionals per a aquest procés sovint utilitzen metalls nobles com el pal·ladi, el ruteni i l'iridi. Tot i la seva efectivitat, aquests metalls presenten desavantatges significatius, com ara la disponibilitat limitada, el cost elevat, de contaminació mediambiental i de toxicitat. Com a conseqüència, hi ha hagut un canvi cap a l'ús de metalls de transició de la primera fila més sostenibles i abundants, amb complexos de ferro emergint com una alternativa prometedora.

La investigació sobre complexos de ferro té com a objectiu millorar l'eficiència d'aquests catalitzadors mitjançant la modificació dels substituents en l'estructura de ciclopentadienona dels catalitzadors de tipus Knölker. Estudis previs han indicat que aquestes modificacions poden reduir les barreres energètiques, millorant així la reactivitat dels catalitzadors. L'estudi se centra en comprendre com aquests canvis estructurals impacten en l'activació del catalitzador i en el pas determinant de la velocitat (rds) en el cicle catalític.

L'activació implica l'alliberament d'un lligand CO facilitat per l'òxid de *N*-trimetilamina, que genera l'espècie activa essencial per al procés catalític. El rds és el pas d'hidrogenació, utilitzant hidrogen molecular, i és notablement exigent en termes energètics. Dissolvents com l'etanol o l'aigua poden ajudar en aquest pas reduint la barrera energètica.

Els resultats revelen que alterar els substituents en l'estructura de ciclopentadienona i l'anell conjugat redueix significativament les barreres energètiques, millorant així l'eficiència catalítica. Els anàlisis computacionals, incloent avaluacions d'índexs electrònics i geomètrics com les càrregues atòmiques, els ordres d'enllaç de Mayer i les funcions de Fukui, proporcionen informació sobre la reactivitat i els patrons d'interacció dins de l'estructura del catalitzador. Els mapes estèrics ofereixen representacions visuals de l'arranjament espacial del catalitzador i les seves interaccions amb els substrats, aclarint més els efectes de les modificacions estructurals en el rendiment catalític.

En conjunt, l'estudi demostra que les modificacions estructurals en els catalitzadors basats en ferro poden influir directament en les barreres energètiques del cicle catalític, afectant així l'eficiència del procés d'hidrogenació i les condicions sota les quals es pot dur a terme la síntesi dels complexos.

Resumen

La hidrogenación catalítica, es vital en las industrias químicas y farmacéuticas. Los catalizadores tradicionales suelen usar metales nobles como paladio, rutenio e iridio, que aunque efectivos, tienen desventajas significativas: disponibilidad limitada, alto costo y preocupaciones ambientales y de toxicidad. Por ello, se está explorando el uso de metales de transición de la primera fila, más sostenibles y abundantes, destacándose los complejos de hierro como una alternativa prometedora.

La investigación sobre complejos de hierro busca mejorar la eficiencia de estos catalizadores mediante la modificación de los sustituyentes en la estructura de ciclopentadienona y el anillo anulado de los catalizadores de hierro tipo Knölker. Se ha demostrado que tales modificaciones pueden reducir las barreras energéticas y, por ende, mejorar la reactividad de los catalizadores. Este estudio se centra en comprender el impacto de estos cambios estructurales en la activación del catalizador y en el paso determinante de la velocidad (rds) en el ciclo catalítico.

La activación del catalizador implica la liberación de un ligando de CO facilitada por el óxido de N-trimetilamina, generando la especie activa esencial para el proceso. El rds, el paso de hidrogenación usando hidrógeno molecular, es altamente demandante en términos energéticos. Disolventes como etanol o agua pueden reducir esta barrera energética.

Los resultados muestran que modificar los sustituyentes en la estructura de ciclopentadienona reduce significativamente las barreras energéticas, mejorando la eficiencia catalítica. Los análisis computacionales, que incluyen evaluaciones de índices electrónicos y geométricos como las cargas atómicas, los órdenes de enlace de Mayer y las funciones de Fukui, proporcionan información sobre la reactividad y los patrones de interacción dentro de la estructura del catalizador. Los mapas estéricos ofrecen representaciones visuales de la conformación espacial del catalizador y sus interacciones con los sustratos, aclarando cómo las modificaciones estructurales afectan el rendimiento catalítico.

En resumen, el estudio demuestra que las modificaciones estructurales en los catalizadores basados en hierro pueden influir directamente en las barreras energéticas del ciclo catalítico, mejorando la eficiencia del proceso de hidrogenación y las condiciones de síntesis de los complejos.

Abstract

Catalytic hydrogenation, is a crucial process in the chemical and pharmaceutical industries. Traditional catalysts for this process often use noble metals like palladium, ruthenium, and iridium. Despite their effectiveness, these metals pose significant drawbacks, including limited availability, high cost, and environmental and toxicity concerns. Consequently, there has been a shift toward using more sustainable and abundant first-row transition metals, with iron complexes emerging as a promising alternative.

The research on iron complexes aims to enhance the efficiency of these catalysts by modifying the substituents on the cyclopentadienone structure of Knoölker-type iron catalysts. Previous studies have indicated that such modifications can lower energetic barriers, thereby improving the reactivity of the catalysts. The study focuses on understanding how these structural changes impact the activation of the catalyst and the rate-determining step (rds) in the catalytic cycle.

In this context, the activation involves the release of a CO ligand facilitated by trimethylamine-*N*-oxide, which generates the active species essential for the catalytic process. The rds is the hydrogenation step, mediated by molecular hydrogen, and it is notably energy-demanding. Solvents like ethanol or water can assist this step by reducing the energy barrier.

The results reveal that altering the substituents on the cyclopentadienone and the annulated-ring structure significantly reduces the energy barriers, thereby enhancing catalytic efficiency. Computational analyses, including evaluations of electronic and geometric indices such as atomic charges, Mayer Bond Orders, and Fukui functions, provide insights into the reactivity and interaction patterns within the catalyst structure. Steric maps offer visual representations of the catalyst's spatial arrangement and interactions with substrates, further clarifying the effects of structural modifications on catalytic performance.

Overall, the study demonstrates that structural modifications in iron-based catalysts can directly influence the energy barriers of the catalytic cycle, thereby affecting the efficiency of the hydrogenation process and the conditions under which the synthesis of the complexes can occur.

ETHICAL REFLECTION

Ethical considerations in computational chemistry, which is the focus of my thesis, are crucial due to the impact on society and the environment. This field uses techniques to understand the properties of molecules and chemical reactions, raising issues such as the ethical use of information, research transparency, and access to knowledge. It is vital to avoid the appropriation of ideas and plagiarism by clearly disclosing the methods used to ensure credibility. Additionally, it is essential that the information is used for positive purposes to advance towards free and better knowledge for all. In summary, computational chemistry offers significant advancements but also presents ethical challenges that require responsibility and honesty.

SUSTAINABILITY REFLECTION

This project utilized supercomputers for calculations. Unlike experimental chemistry, this procedure required no tangible materials or waste. However, environmental factors, including the management of energy, must be considered in scientific research. Many tons of harmful materials are used globally each day, and despite neutralization methods, the issue persists. While computational chemistry avoids this problem by relying solely on computers, the energy consumption of these powerful machines must be considered for the prevention and control of pollution. There are ways to mitigate this energy use without harmful materials and it needs to be taken into consideration for the future research.

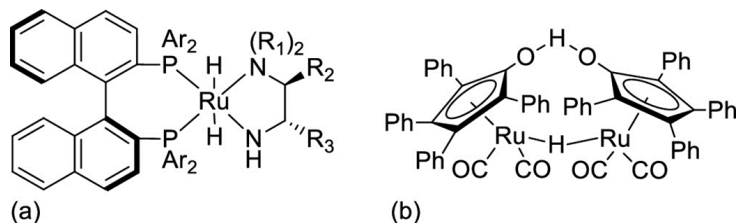
GENDER PERSPECTIVE REFLECTION

The gender perspective in chemistry, especially in physical chemistry, is crucial. Despite advances, sciences have been dominated by men, as shown by Rosalind Franklin's case in the DNA discovery by Watson and Crick. Fortunately, women's roles are gaining prominence, as seen at the University of Girona. The Faculty of Sciences has almost parity, but in the Department of Chemistry, men outnumber women¹. In my research group, women are significantly represented but do not reach 50%. In fact, a man and a woman supervise this work. The underrepresentation of women is attributed to abandoning scientific careers due to a lack of job stability, the pressure to start a family, and the impact of microaggressions. This issue reflects the glass ceiling, a societal difficulty in achieving high-level positions and salary equality. A paradigm shift with equitable education and institutional support is needed.

¹Dades extretes de *Dades desgregades 2022-2023*. Consultat el dia 07/06/2024.
<https://www.udg.edu/ca/Portals/50/Igualtat/DADES%20DESAGREGADES%2022%2023%20Web.pdf?ve r=4rd9tLLbGaaao3txXZ2kgQ%3d%3d>

1 Introduction

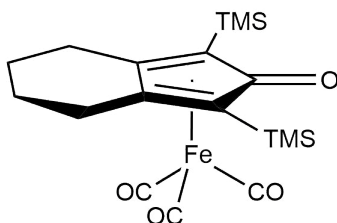
In the chemical and pharmaceutical industry, the catalytic hydrogenation of double bonds between homoatoms or heteroatoms has taken a lot of importance [1]. Moreover, the academic research world has heightened its interest in studying this type of reactions. During the last years, the imine reduction mechanism has been carried out by noble transition metals such as palladium, ruthenium, or iridium [2]. This type of metals have shown huge efficiency in reductive amination. Amongst these metal catalysts, the ruthenium complexes are the long-established ones. To be specific, Noyori [3] and Shvo [4] catalysts have been used for that purpose (Scheme 1).



Scheme 1: Noyori (a) and Shvo (b) catalysts.

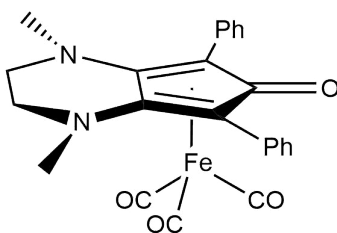
The noble-metal-based catalysts present inherent problems due to their low earth abundance, low stability, and toxicity. So, the trend of replacing this type of metal with more sustainable ones has recently gained interest. One of the most reliable options that have been proposed in the literature falls in the first-row transition metals regime. In particular, iron complexes have been highly used due to their easy manipulation and affordability.

Over the past years, related iron complexes have received some attention. Casey *et al.* [5] reported that the (cyclopentadienone)iron tricarbonyl complexes can catalyse the reduction of carbonyl substrates, the so-called Knölker-type catalysts (Scheme 2) [6]:



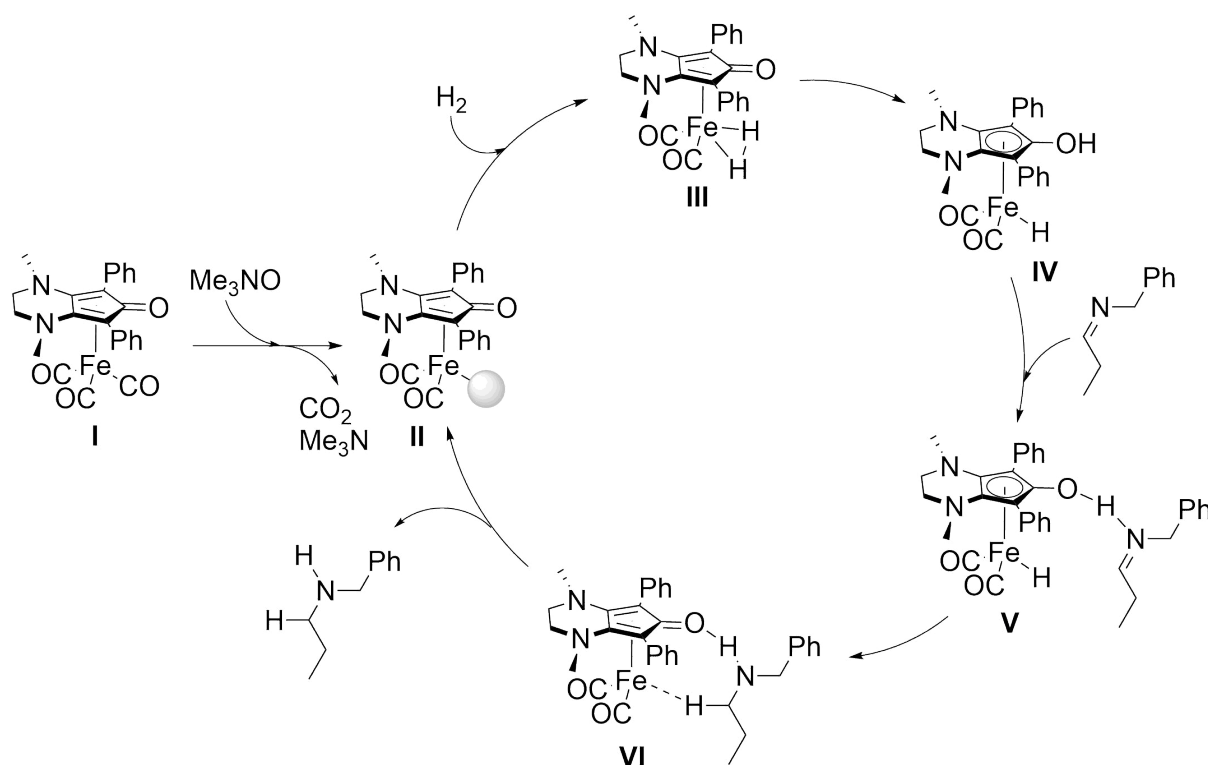
Scheme 2: Knölker catalyst.

Recent studies from Poater and Renaud [7] have show that modifying the substituents of the cyclopentadienone structure substantially decreases the energetic barriers, hence improving the reactivity and enhancing the chemoselectivity of the catalytic hydrogenation (Scheme 3).



Scheme 3: Renaud catalyst.

Several well-established studies carried out by Beller *et al.* [8] prompted Poater and Renaud to modify this family of catalysts in order to enable the catalysis of reductive amination of carbonyl compounds by using molecular hydrogen as a reducing agent (Scheme 4).

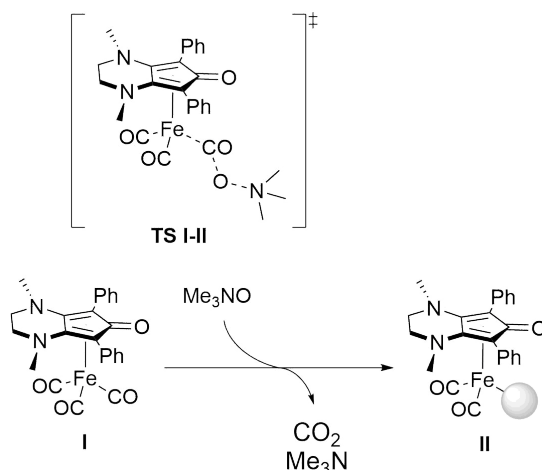


Scheme 4: General scheme for the C=N bond hydrogenation using Renaud catalyst.

The catalytic cycle for reductive amination using Renaud complex involves several key steps. Initially, the catalyst is activated through a reductive elimination with trimethylamine-*N*-oxide to form the catalytic active species **II** which has an energy cost of 19.6 kcal/mol. The next step involves the reaction of intermediate **II** with molecular hydrogen to form intermediate **III** through a low-energy transition state (**II-III**). Subsequently, **III** forms iron hydride **IV** with a significant energy barrier through transition state **III-IV**. In this step, one hydrogen atom is transferred from the π -coordinated H_2 to the C=O group of the cyclopentadienone. Following this, in the presence of an imine, hydrogenation occurs to form the corresponding secondary amine, leading to intermediate **VI**. The final step involves the release of the amine formed, regenerating intermediate **II**, and closing the catalytic cycle.

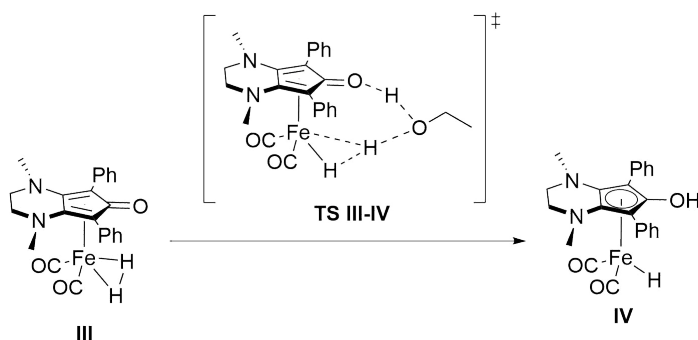
It was reported that the rate-determining step (rds) of the catalytic cycle was the step from **III** to **IV** using H_2 due to the high energy demand (24.4 kcal/mol). Later on, it was found that this reaction step could be assisted by one explicit solvent molecule (either ethanol or water). As a result, the barrier decreases to 14.7 or 17.2 kcal/mol, respectively. This revelation means that the activation of the catalyst by the losing of the CO ligand, from **I** to **II**, requires more energy than the rds of the catalytic cycle.

The first step, as said before, consists of the release of the CO ligand attached to the metal (Scheme 5) using Me_3NO which forms CO_2 and Me_3N .



Scheme 5: Activation of the Renaud catalyst by Me_3NO .

The second studied step uses an explicit ethanol molecule (solvent), as it is less energy-demanding than water, to assist the hydrogen transfer from the π -conjugated hydrogen molecule to the ketone in the cyclopentadienone.



Scheme 6: Hydrogenation of the keto group of the cyclopentadienone of intermediate **III** for Renaud catalyst assisted by an ethanol molecule.

These two reactions are the most energetically demanding and can determine the efficiency of the catalytic cycle. Any alteration in the catalyst's structure would induce changes in these barriers of the cycle, thereby influencing other physicochemical aspects of the reaction that may either favor or hinder catalysis. These two steps in the reaction pathway appear to be crucial. However, they possess fundamentally different natures. The transition from **I** to **II** represents the activation of the catalyst, while the transition from **III** to **IV** constitutes the rds of the catalytic cycle.

For that reason, this study will focus on the computational analysis of these two steps and the variations in kinetic barriers resulting from different modifications of Renaud's catalyst, aiming to enhance our understanding of the catalyst's efficiency and behavior.

This work falls within the scope of predictive catalysis, a branch of computational chemistry that leverages advanced techniques in artificial intelligence and machine learning. Predictive catalysis aims to enhance experimental efforts in developing and optimizing catalytic processes by identifying and mastering key parameters that influence activity and selectivity.

In this context, the methodology used in this study allows for the analysis of how various structural modifications to catalysts affect the catalytic cycle under investigation. This approach not only accelerates the discovery of new catalysts but also provides a deeper understanding of underlying mechanisms, facilitating more rational and efficient catalyst design. This is why the data extracted from this work, along with future data, will be used to feed these neural networks, advancing the field of predictive catalysis.

2 Objectives

In the introduction it has been seen that the study of the modified Knölker-type catalyst could provide lower kinetical barriers for the catalytic cycle. By dint of that, the principal aims of this bachelor thesis are:

- Investigate the behavior of different catalyst structures to identify strategies to lower activation barriers, enabling operation under milder conditions that reduce undesired parallel reactions.
- Analyze the results obtained from the modifications made to the catalyst to understand their impact on catalytic performance.
- Conduct various tests to provide a plausible explanation for the observed results, ensuring a thorough understanding of the catalytic processes involved.

3 Methodology

For the development of this work, the calculations were performed using the program Gaussian 09 [9]. The functional used to perform the calculations was BP86 [10] to optimize geometries. For the calculation of the electronic structure the standard split-valence basis set with a polarization function of Ahlrichs *et al.* for H, C, O, N, F and Si was used (denoted as SVP keyword in Gaussian program) [11]. For the transition metal Fe, Stuttgart/Dresden core pseudo-potential (SDD) was used [12]. With the optimization of geometries, frequencies have been calculated to determine if a minimum on the potential energy surface has been reached. For intermediates, all the obtained frequencies are positive. In the case of transition states, a negative frequency corresponding to the desired vibration has been obtained. Afterwards, all the representations of the analyzed structures were generated utilizing the Chemcraft software [13].

Precise electronic energies were obtained through single-point calculations at M06/cc-pVTZ [14][15] level of theory to describe H, C, O, N, F, and Si, whereas the SDD basis set was used for the Fe atom. For the purpose of improving the modeling of the reaction, ethanol was added as an implicit solvent using the polarizable continuous solvation model (PCM) [16] for the reaction step **III** \rightarrow **IV**.

Several studies have been performed to further understand the energetical differences between the systems, which mainly include aromaticity, the characterization of catalytic pockets as well as other geometrical and electronic indicators such as bond distances, Mayer Bond Orders (MBO), the variation of the atomic charges from the Natural Population Analysis (NPA), and conceptual DFT, in particular by Fukui functions.

3.1 Electronic and geometrical indices

3.1.1 Atomic charges

The atomic charge in a molecule provides valuable insights into the electron density distribution, aiding in the understanding of its structure. Although these charges are not directly observable experimentally, computational methods effectively utilize them to correlate molecular properties with the observed structure.

This study examines the atomic charges of specific regions within the molecule to establish a relationship with the catalyst's reactivity, offering a deeper understanding of how electronic distribution influences catalytic behavior.

3.1.2 Mayer Bond Order (MBO)

In the mid-1980s, Mayer introduced a method for calculating bond orders [17]. His definition was highly successful because it could be extended to extract additional information about orbital contributions to chemical bonds and to address multi-center electronic interactions[18].

In this study, Mayer Bond Orders (MBO) are used to measure the specific reactivity of a given bond. By definition, the computed MBO value indicates the strength or weakness of a bond, providing a quantitative assessment of its reactivity.

3.1.3 Fukui function

Thanks to the conceptual Density Functional Theory (DFT), Fukui functions could be defined as a descriptor that allows the identification of the most reactive sites on a molecule, even for electrophilic or nucleophilic reactions. This indicator measures the electron density induced by the change of absolute electron number with fixed geometry and potential. As a way to determine the local reactivity of an atomic center, condensed Fukui functions were introduced by Yang *et al.* [19].

The function is defined as the change of the charge that undergoes a determined atom in relation to the change of the total number of electrons in the molecule (Equation 1).

$$f_k = - \left(\frac{\partial q_k}{\partial N} \right)_{\nu(r)} \quad (1)$$

Because of the definition, natural population analysis (NPA) must be used.

For this work, the considered definition of the condensed Fukui function at the atom k (f_k^-) follows as

$$f_k^- = [q_k(N-1) - q_k(N)] \quad (2)$$

where q_k indicates the electronic charge on atom k in a system with $(N-1)$ and (N) electrons calculated without changing the symmetry. Therefore, f_k^- describes the capacity of an atom to deal with an electrophilic attack by removing an electron from the molecule.

3.2 Steric maps

In 2016, Falivene *et al.* [20] introduced a new web server with the capacity to generate steric maps through the concept of $\%V_{Bur}$ [21], designed to quantify differences in catalytic pockets and correlate the experimental behavior of a catalyst with its structure. This tool utilizes the concept of topographic steric maps, which serve as physicochemical analogs to physical maps in geography. These maps offer a visual representation of the interaction surface between the catalyst and its substrates, shaped by the ligands within the complex.

To achieve this, the optimized structures were converted into XYZ files and processed using the web server. To observe the catalyst's structure and its impact on the reaction center (the metal), the central point was focused just below the metal. To generate the coordinate axes, the two most distant carbon atoms from the cyclopentadienone are selected as the z-axis. The oxygen atom of the ketone group is chosen to define the xz plane. This method ensures a clear depiction of the catalyst's structure, minimizing potential interferences when creating the topographic map. This approach allows for a detailed visualization of the spatial arrangement and interactions within the catalytic system, providing valuable insights into how the catalyst's geometry influences its activity and effectiveness.

3.3 Aromaticity

The aromaticity of a given chemical system is highly related to its stability and reactivity. Even though its importance in the chemistry field, it holds one major drawback: “*No single property exists that could be taken as a direct measure of aromaticity*” [22]. Therefore, many scientists have evaluated the use of various aromaticity descriptors derived from different criteria. In computational chemistry, aromaticity indices could be assorted into three distinct categories: geometric, electric, and magnetic. This work only focuses on the formers, which are called intrinsic indexes because they measure intrinsic properties of the molecules themselves, properties that show without any external perturbation.

The indexes used here were I_{ring} , I_{NG} , MCI, I_{NB} , FLU, BOA, BLA, PDI and HOMA [23][24].

HOMA

Harmonic oscillator model of aromaticity (HOMA) [25], is a geometric index, and it relies on the similitude between the bond distances studied in the molecule to a reference one and also on the alternation of this bond-length. The biggest limitation of this descriptor is the dependence on reference values because there are very few of it (C–C, C–N, C–O, C–P, C–S, N–N, N–O). If HOMA value is nearby to 1, it means that the species is aromatic. For small or negative values, it indicates an antiaromatic or non-aromatic species.

I_{ring}

Giambiagi *et al.* [26] generalized the delocalization index concept to multiple atomic centers, and later on proposed this concept as a measure of aromaticity. From this proposal emerged a new descriptor, the I_{ring} . This multicenter index quantifies the electron delocalization along the ring, thanks to the Kekulé contributions. The value of the I_{ring} depends on the size of the studied ring, so later on, Cioslowki *et al.* proposed the normalized version, the I_{NG} [27]. Large values arise from aromatic molecules.

MCI

In order to improve the I_{ring} , Bultinck and coworkers proposed to take into account all the delocalization patterns across the ring and combine them [28]. Overall, is the sum of all possible permutations of the delocalization patterns in a ring. Also as in I_{ring} , Cioslowki proposed the normalized version to compare different structures, I_{NB} [27]. Large values of MCI are characteristic of aromatic molecules, nevertheless, antiaromatic molecules often give negative values.

FLU

The fluctuation index (FLU) is an electronic index [29]. That is because only employs the electronic delocalization of the atoms in the ring and compares them with the cyclic electron delocalization of an aromatic molecule reference. If their values are close to 0 means an aromatic behavior, as the delocalization is similar to the reference one. Large FLU values mean nonaromatic or antiaromatic species.

BOA

The bond-order-alternation (BOA) compares the bond order or electron-sharing index of consecutive bonds. This descriptor depends much less on the method and the basis set used. BOA assumes values near 0 for aromatic molecules.

BLA

Bond-length alternation (BLA) is a geometric index, that compares the average of bond lengths of consecutive bonds in a ring or conjugated chains, denoting that the value of this descriptor depends on the dominance of the resonant structures drawn from the conjugated form. A value near 0, reveals an aromatic behavior on the chain or ring studied.

PDI

Fulton [30] and Bader [31] showed that benzene has larger delocalization indices between the atoms in para position than in meta position. That's why Poater *et al.* defined the para-delocalization index (PDI) [32], which is an average of the delocalization indices between atoms in para position in a six-membered ring. Larger values of PDI mean greater aromatic behaviour.

In the presentation of the various indices, the properties of the different structural rings will be highlighted. Therefore, when studying the aromatic properties of the compounds in this work, the criteria outlined in Figure 1 will be followed.

The first ring will always be the cyclopentadienone, and the second will be the central ring, whether it is the cyclohexane in Knölker complexes or the heterocyclic ring in Renaud-based catalysts. This approach is adopted to facilitate the comparison of structures with and without the fused ring.

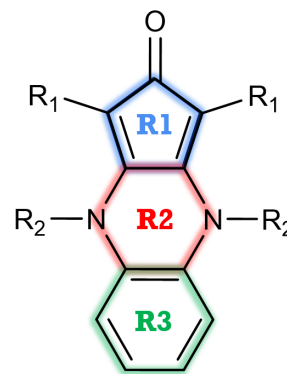


Figure 1: Criteria for studying the aromaticity of the catalysts.

4 Results and discussion

4.1 Scope of catalysts by predictive chemistry

The study of different structures could determine the success of the objectives. For that purpose, the structures were determined by taking into account the following statements:

- Examine how the presence of various electron-withdrawing (EWG) and electron-donating (EDG) substituents affects the reactivity and stability of ligands.
- Introduction of a third annulated ring, aromatic, next to the 6 membered ring also annulated to the 5-membered ring of the cyclopentadienone.

As previously stated, Poater and Renaud, inspired by the ‘‘Frustrated Lewis Pair’’ (FLP) approach [33], proposed modifications to the ligands to achieve two goals: increasing the Lewis acidity of the iron atom and enhancing the basicity of the carbonyl group on the cyclopentadienone ligand. Since CO ligands are known to be highly π -acidic, their efforts were directed towards altering the cyclopentadienone structure (Figure 2).

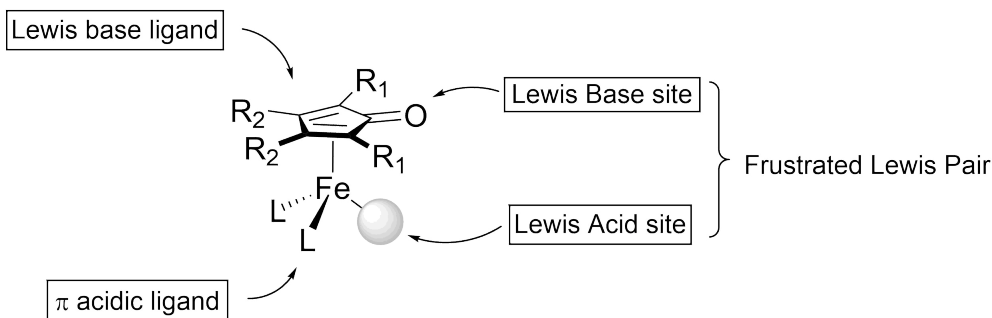


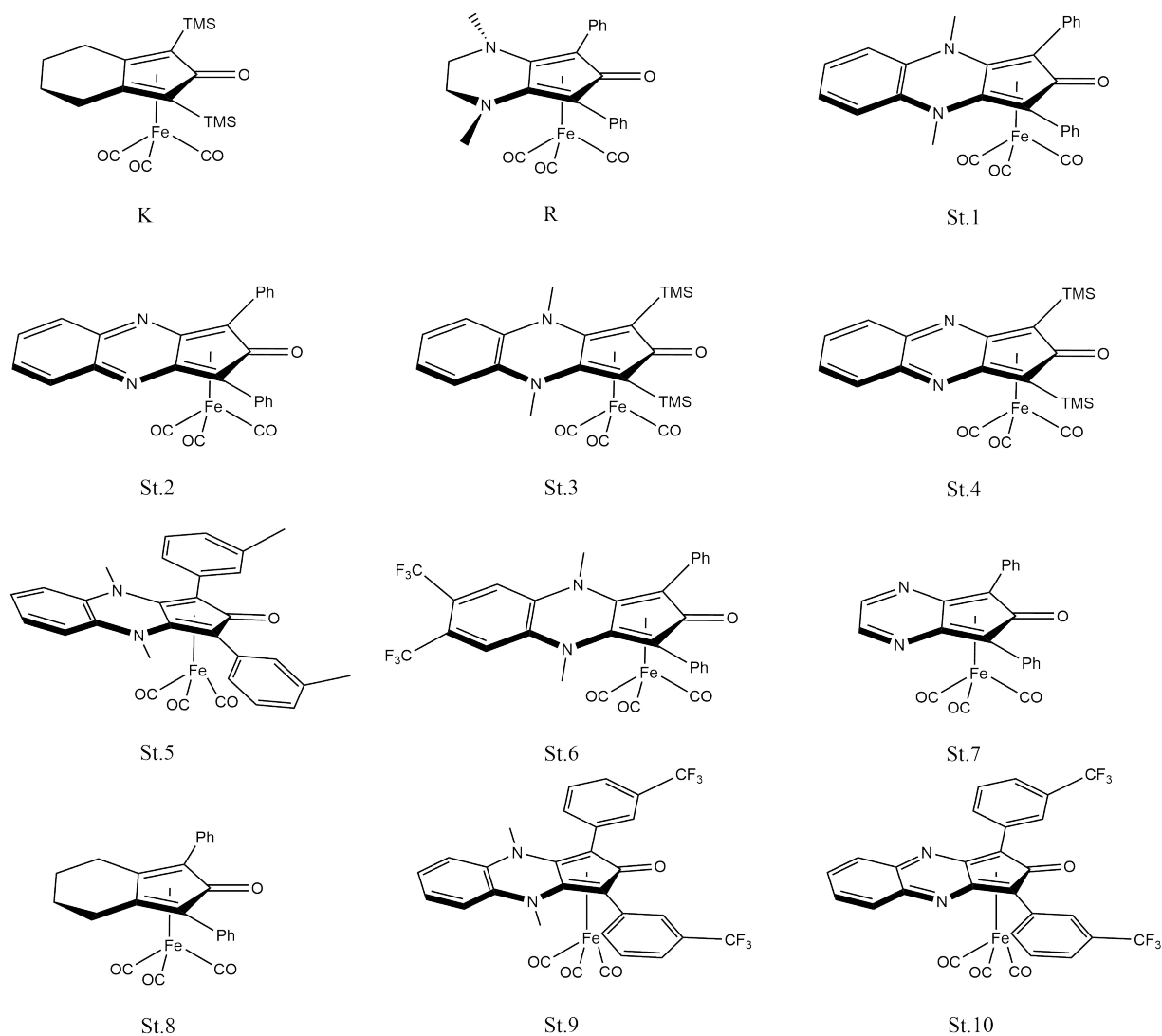
Figure 2: Frustrated Lewis Pairs sites in the main structure of the catalysts.

Upon determining the compound’s nature and pinpointing potential modification sites, the focus shifts to identifying alterations that could effectively modulate energy barriers within the catalytic cycle. Thence, the first change with respect to the original Renaud catalyst (Scheme 3) is to add an annulated benzene ring as a Lewis base ligand.

The inclusion of a benzene ring in the structure contributes to its aromaticity, making modifications to this aspect particularly interesting. Additionally, the presence or absence of the amino methyl group could significantly impact the aromatic structure due to the potential loss of the aromaticity provided by the benzene ring.

Also it was reported that the substituent of the cyclopentadienone could modify the energy barriers. DFT calculations conjoined to the effective oxidation state (EOS) analysis makes it possible to conclude that the presence of electron-withdrawing ligands (*i.e.*, CF_3) produce a decrease of the barriers in comparison with the electron-donating ones.

For that reasons, and with the strenghten by the backing of experimental research groups, the following structures have been studied (Scheme 7).



Scheme 7: Representation of computed chemical structures.

The initial structures analyzed were the Knölker (K) and Renaud (R) catalysts, available yet experimentally. These were chosen due to their well-documented performance in previous studies and to provide a baseline for comparison with newly developed catalysts. To further understand the impact of structural modifications, their altered versions, St.7 and St.8, were also examined, focusing on the effects of introducing methyl and phenyl substituents to the original frameworks.

Building on this foundation, further modifications led to the development of structures St.1 to St.4. These modifications aimed to enhance catalytic performance and explore the effects of different substituents and structural changes. Based on the promising results from these initial experiments, and informed by the detailed study conducted by Joly *et al.* [7], additional structures, St.5, St.9, and St.10, were proposed. These new structures aimed to further refine the catalysts' efficiency and selectivity.

Lastly, to ensure a comprehensive understanding of various influencing factors, structure St.6 was introduced. This structure was specifically designed to study the impact of electron-withdrawing groups (EWG) on the six-membered aromatic ring, offering insights into how these groups affect the overall catalytic activity and stability. Through these systematic studies and modifications, a robust framework for catalyst development was established, providing valuable insights into the relationships between structure and function.

The comprehension and analysis of the original and the proposed catalysts create a basis for understanding the foundations of how the structure modifies the energy barrier of the catalytic cycle.

As we are interested in the study of the catalytic cycle regarding reductive amination catalysis, specifically the imine to amine reduction, we will study the reactions with the most heightened energy profile from a kinetic point of view.

The initial phase of our investigation will center on conducting studies concerning structural parameters. Our aim is to gain a deeper understanding of the mechanisms underlying reactions and identify the predominant factors.

Subsequently, we will conduct further investigations to examine how structural modifications impact energy barriers, particularly concerning aromaticity issues when comparing Knölker’s and Renaud’s derivative catalysts.

4.2 Kinetic cost

The first set of calculations performed was obtaining the kinetic barriers of the different catalysts at the given reactions. We will focus on previously stated modifications and how the activation energy changes (ΔG), the values of which are gathered in Table 1.

Table 1: Energy barriers (ΔG) for the studied structures for the steps **I** \rightarrow **II** and **III** \rightarrow **IV**, in kcal/mol.

	K	R	St.1	St.2	St.3	St.4	St.5	St.6	St.7	St.8	St.9	St.10
I \rightarrow I-II	18.4	20.6	17.4	9.3	24.2	14.9	18.8	17.8	10.2	15.5	17.2	10.2
III \rightarrow III-IV	12.5	16.0	13.1	9.8	20.7	11.4	16.2	15.0	11.0	13.9	15.6	10.3

At first glance, one can see that the activation energy of both Knölker (K) and Renaud (R) catalysts are quite energy-demanding with values from 12.5 to 20.6 kcal/mol. The barrier coming from Knölker’s catalysts has been shown to be smaller than that of Renaud, even though the difference between them is not that vast.

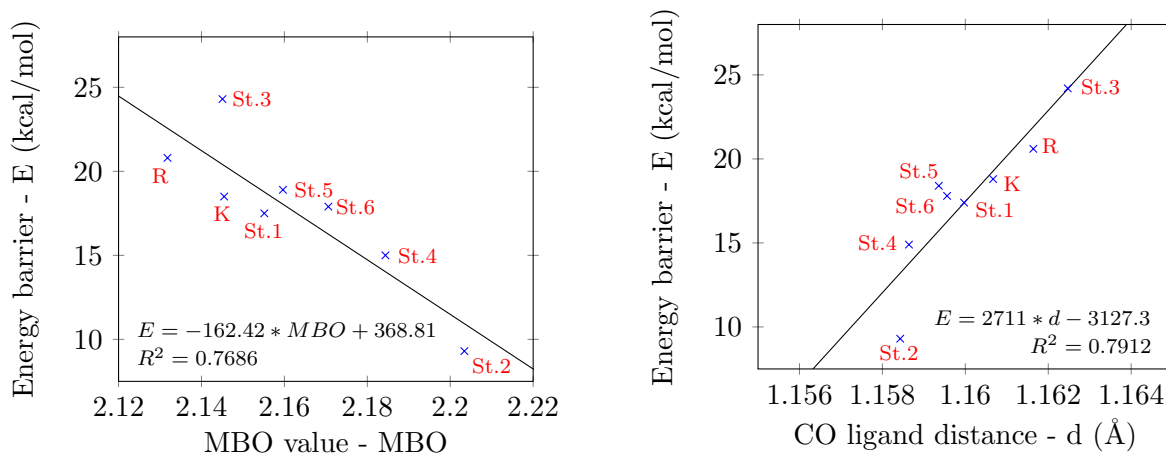
As we were interested in the catalysts that improve those reactions that use Knölker and Renaud, the same calculations were performed using the modified version of the previous systems.

The results show that generally all ΔE_a are below the reference values, except for the St.3 system which has higher barriers. The set of modification that drastically improves the energy requirements is St.2, the values of which fall under 10 kcal/mol, proving a huge significance with respect to both the reference system and the other modifications. As for the other systems, while some of them improve the performance of the reaction, some others stay higher in energy. Hence, these catalysts improve the reference ones but are not as good as St.2.

Hereafter, we will discuss all the applied modifications to Renaud’s catalyst, making emphasis in the electronic structure, reactivity and aromaticity, and how these affect the kinetic energy profile.

4.3 Structural characterisation

In the specific reaction step from **I** to **II**, the critical factor driving the reaction is the dissociation of a CO ligand from the metal by Me_3NO that consequently releases CO_2 and Me_3N molecules. This significant step marks a key transformation within the reaction mechanism. Consequently, indicators of this formation include the Mayer Bond Order (MBO) and the bond distance of the carbonyl group, which is released during the activation of the catalyst. These parameters are crucial as they provide insights into the structural changes and energetic requirements of the reaction, helping to better understand the catalytic process (Figure 3).



(a) Relationship between the MBO values of the CO ligand and the activation barrier.

(b) Influence of the CO ligand bond length on the activation barrier.

Figure 3: Comparative analysis of MBO values and CO bond length in relation to the activation barrier for intermediate **I** in Gibbs energies.

The negative slope of Figure 3a indicates that as the bond order increases, the energy barrier of the reaction decreases. This phenomenon can be explained by the stabilization of the carbonyl ligand as it transitions into CO_2 . The formation of CO_2 involves a double bond with the other oxygen atom, resulting in a more stable configuration.

Furthermore, the graph depicting the bond distance between the two involved atoms (Figure 3b) reveals that as the bond distance increases, the reaction encounters greater activation energy. This trend, when considered alongside the Mayer Bond Order (MBO), suggests that the minimum energy distance for the formation of CO_2 is shorter than the bond distance when the carbonyl group is bonded to the Fe atom as a ligand. The shorter bond distance is energetically more favorable for the formation of CO_2 , thereby reducing the energy barrier for the reaction.

Additionally, the increase in bond distance reflects a state where the reaction is less likely to proceed, as it moves away from the optimal conditions required for CO_2 formation. This is consistent with the MBO values, indicating that higher bond orders and shorter bond distances are conducive to a more efficient catalytic process, ultimately leading to a lower energy barrier for the reaction. These insights are crucial for understanding the dynamics of the reaction and the role of bond distances and orders in influencing the energy landscape of the catalytic process.

Another potentially key factor is not the distance from trimethylamine-*N*-oxide to the complex, but rather the distance between the metal and the carbonyl ligand and the distance between

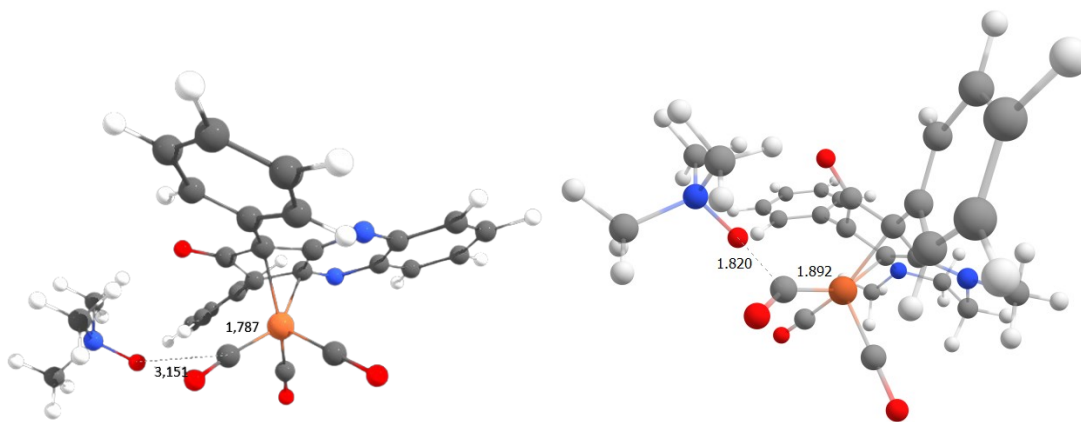
the carbon in the CO ligand and the oxygen from the Me₃NO (Table 2).

Table 2: Distances for the Fe–C bond, ligand C–O and C–O distance between Me₃NO and ligand in **I** intermediate and transition state **I-II** of some molecules summarized in Scheme 7. Units are in Å.

		K	R	St.1	St.2	St.3	St.4	St.5	St.6
I	Fe–C	1.795	1.797	1.804	1.775	1.798	1.776	1.806	1.807
	C–O (ligand)	1.159	1.162	1.160	1.158	1.163	1.159	1.161	1.160
I-II	Fe–C	1.879	1.892	1.885	1.787	1.906	1.845	1.888	1.892
	C–O (ligand)	1.185	1.188	1.179	1.158	1.194	1.181	1.179	1.180
	C–O (ligand-Me₃NO)	1.188	1.820	1.954	3.151	1.742	1.947	1.981	1.942

Thanks to Table 2, a trend can be predicted where higher activation energy values correspond to longer bond distances between the iron and the ligand. When considering the distance between carbon and oxygen, a notable trend is also observed where a greater distance leads to a reduced kinetic barrier.

As shown in Figure 4a, which depicts the St.2 catalyst, the distance between the oxygen of Me₃NO and the carbon of the CO ligand - eventually transforming into the carbon dioxide to be released - is relatively long (3.151 Å). Despite this, the energy barrier is the lowest among all the structures studied. This can be explained because it is the least distorted structure and also because the steric hindrance suffered by the Me₃NO moiety is less than for any of the other studied systems.



(a) Transition state **I** → **II** of catalyst St.2. (b) Transition state **I** → **II** of Renaud catalyst.

Figure 4: Transition state **I** → **II**. Selected distances are shown in Å.

This observations aligns with the charge values of both the carbon in the ligand and the iron, as shown in Table 3.

Table 3: NPA charges for the Fe and ligand's C atoms in **I** intermediate of some molecules summarized in Scheme 7. Units are in e.

	K	R	St.1	St.2	St.3	St.4	St.5	St.6
qFe	-1.509	-1.528	-1.492	-1.350	-1.502	-1.393	-1.507	-1.510
qC	0.928	0.905	0.903	0.938	0.897	0.946	0.9013	0.905

A noticeable trend emerges from the data. Due to the electronic effects within the system, when the metal acquires more negative charge from the structure, part of this charge is transferred to the ligand, making it more labile and causing it to position further away from the metal. These effects stabilize the transition state during the reaction, resulting in a lower activation energy for the catalyst.

This relationship highlights the importance of both bond length and atomic charges in understanding and predicting the reactivity of the catalytic system.

This relationship is justified by the first intermediate (**I**), indicating the catalyst’s activation. The same reasoning can be applied to the second reaction studied in this work.

As previously mentioned in the methodology, one of the key indicators for understanding changes in the energy barrier are the Fukui functions. In the context of this study, these functions provide insight into how effectively an atom responds to an electrophilic attack. Specifically, during the transition from **III** to **IV**, when H_2 interacts with the oxygen atom of the keto group in cyclopentadienone, facilitating the transfer of hydrogen. By definition of the function, we will apply this study to the oxygen atom of the ketone group in intermediate **III** as it is the site expected to receive the electrophilic attack from the hydrogen coordinated with the metal. This specific focus is crucial because the interaction between the ketone oxygen and the hydrogen plays a fundamental role in the catalytic mechanism. Understanding this interaction will provide deeper insights into the reactivity and efficiency of the catalyst, potentially guiding future modifications to enhance catalytic performance.

In evaluating this process, the absolute values obtained from the Fukui functions may not be as critical. Rather, the variation in these values offers a more accurate representation of the structure’s susceptibility to hydrogen attack. To illustrate this, the following plot (Figure 5) depicts how the energy barrier changes in relation to the different values of the Fukui indices obtained in the study. This approach allows for a more accurate understanding of the factors influencing the energy barrier and provides clearer insights into the reactivity of the molecules involved.

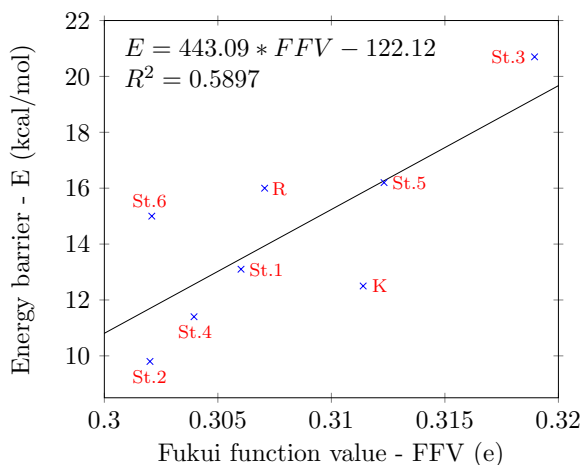
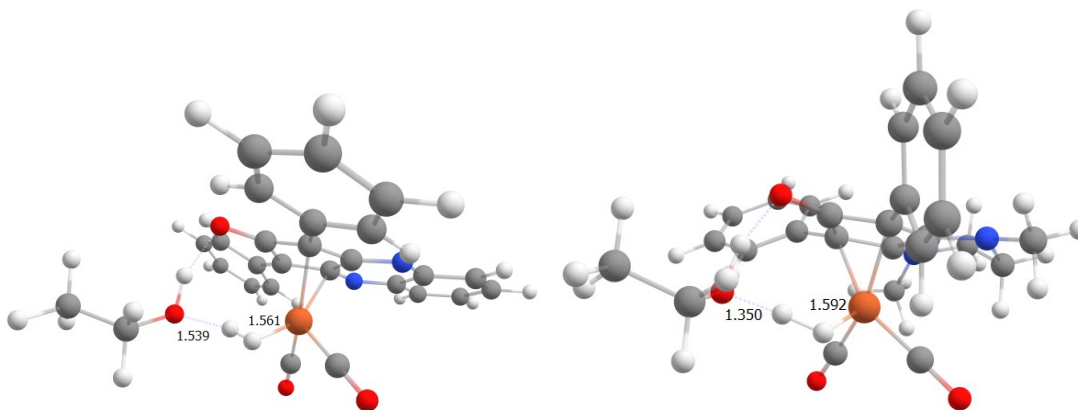


Figure 5: Relationship between the Fukui function values of the oxygen in the keto group and the activation barrier.

When observing Figure 5, a certain trend appears, although it does not correlate perfectly as indicated by the R^2 value. This difference suggests that the Fukui index does not fully explain the observed energy barrier variations. The limitations in the correlation imply that additional factors or variables might influence the energy barrier changes that the Fukui index does not account for.

Another important aspect to consider, as before, is the distances between the molecules involved in the reaction. In this case, we have the distance between the metal and the π -conjugated hydrogen molecule, as well as the distance between the oxygen of the implicit ethanol molecule assisting the reaction and the hydrogen atom that will depart from the metallic center (Figure 6 - Table 4).



(a) Transition state **III** \rightarrow **IV** of catalyst St.2. (b) Transition state **III** \rightarrow **IV** of Renaud catalyst.

Figure 6: Transition state **III** \rightarrow **IV**. Selected distances are shown in Å.

Table 4: Distances for the Fe-H bond in **III** intermediate and H-O distance between the H₂ and EtOH and H-O distance between EtOH proton and the O atom in the ketone group for the transition state **III-IV** of some molecules summarized in Scheme 7. Units are in Å.

		K	R	St.1	St.2	St.3	St.4	St.5	St.6
III	Fe-H	1.636	1.654	1.663	1.613	1.689	1.613	1.669	1.667
	Fe-H	1.588	1.592	1.620	1.561	1.603	1.563	1.616	1.612
III-IV	H-O (H - EtOH)	1.397	1.350	1.341	1.539	1.328	1.536	1.332	1.348
	H-O (EtOH - keto)	1.494	1.401	1.412	1.610	1.374	1.569	1.432	1.441

Thanks to Table 4, we can also observe a certain reduction in the energy barrier when the hydrogen molecule is closer. This reasoning is likely more electronic than steric, due to the proximity of the small molecule and steric hindrance by the catalyst. Additionally, by examining the distance between the molecular hydrogen and the oxygen of ethanol, we also see a behavior where a greater distance results in a lower energy barrier. This behavior can be explained a little by steric factors: being farther apart allows the complex to occupy less crowded space, thus providing more room for the reaction to occur.

4.4 Steric maps

Until now, the focus has been on intrinsic parameters of the catalyst itself, such as bond distance and strength. However, these are not the only structural aspects considered. We have also

examined the steric map of the studied catalyst, particularly around the metal center, to assess the steric hindrance affecting its reactivity. This factor could significantly influence the variations in energy barriers observed during catalytic processes.

In addition to these intrinsic properties, understanding the spatial arrangement around the active site is crucial. By analyzing the steric environment, we can gain insights into how the surrounding ligands and substituents impact the accessibility and efficiency of the catalyst. This comprehensive approach allows for a more detailed understanding of the catalyst’s behavior and potential improvements in its design.

The procedure outlined in the methodology section was meticulously followed to compute the catalytic pockets of the various structures. The different topological maps obtained for the structures of the first intermediate (**I**) are presented in Figure 7. These maps provide valuable visual representations of the steric landscapes, helping to identify areas of potential steric clash or accessibility that could affect catalytic performance.

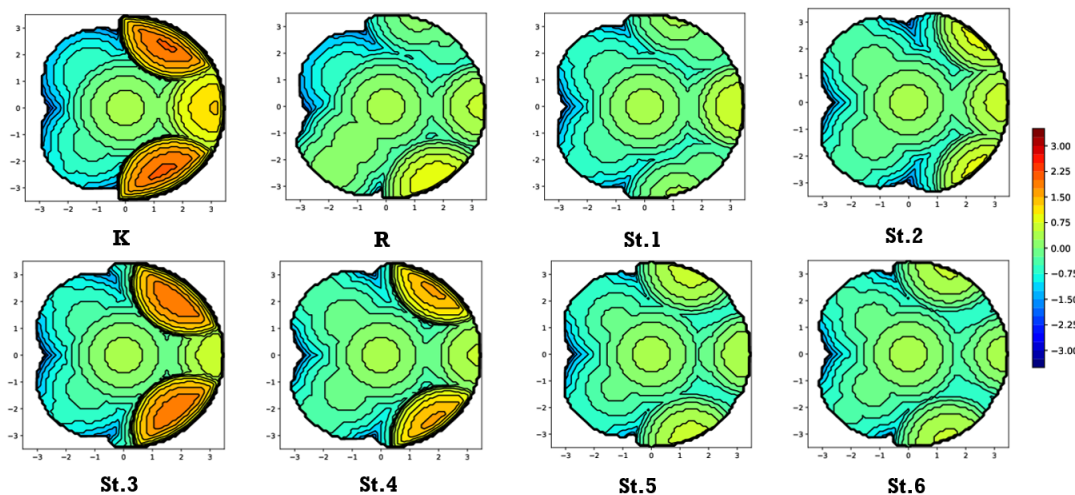


Figure 7: Steric maps (plane xy) of the intermediate **I** for the studied iron complexes, with a radius of 3.5 Å. The metal center of the catalysts are at the origin. The isocontour curves of the steric maps are given in Å.

In this case, we are interested in examining the spatial occupancy around the Fe center, as the approach of Me_3NO - a relatively middle-size molecule compared to the catalytic center - requires sufficient space to facilitate the reaction and subsequent CO_2 release. When comparing pairs of structures (St.1 with St.2 and St.3 with St.4), it is evident that the latter structures exhibit greater steric congestion on the eastern side, where the two substituents in alpha to the keto group of the cyclopentadienone are located, which is the entry point for the Me_3NO molecule. This increased congestion results in a higher energy barrier due to greater steric hindrance, thus reducing the ease of CO_2 release.

For structures St.5 and St.6, it is not clear that the difference in kinetic barriers is due to steric hindrance, as their steric environments are quite similar to other structures with lower activation energies. This suggests that other factors might be contributing to the observed differences in reactivity.

The conclusions remain consistent when focusing on the second step, **III** \rightarrow **IV** studied instead of the first intermediate for catalyst activation (see Figure A1). The various values obtained

for both intermediates are presented in Table 5. These values comprehensively compare steric effects and their impact on the catalytic process.

Table 5: $\%V_{bur}$ of intermediates **I** and **III** for the studied catalysts (total and by quadrants; SW=south-west, NW=north-west, NE=north-east, SE=south-east).

	I					III				
	SW	NW	NE	SE	TOTAL	SW	NW	NE	SE	TOTAL
K	38.4	36.2	71.1	72.0	54.4	38.5	38.5	74.1	74.1	56.3
R	47.0	36.3	48.2	56.0	46.9	43.3	38.9	50.0	52.2	46.1
St.1	39.3	39.3	50.3	50.3	44.8	39.9	39.9	51.3	51.3	45.6
St.2	41.3	41.4	50.5	50.6	46.0	41.6	41.6	51.4	51.4	46.5
St.3	38.1	38.1	67.6	67.6	52.8	39.2	39.1	70.8	70.8	54.9
St.4	41.4	41.4	58.8	58.8	50.1	41.9	41.9	62.6	62.6	52.3
St.5	40.9	40.8	51.6	51.6	46.2	41.9	41.9	51.7	51.7	46.8
St.6	41.5	41.2	50.0	50.1	45.7	42.0	42.2	50.6	50.5	46.3

As observed in Table 5, and considering the energy barriers for these species, a certain trend appears to emerge: greater steric hindrance correlates with higher energy required to overcome the corresponding energy. As mentioned earlier, this explanation likely arises in part from the more obstructed access to the catalytic center in some structures compared to others.

However, while steric hindrance is not the only determinant in predicting this kinetic barrier, it remains a significant factor to consider when modifying catalysts to achieve more favorable reaction conditions. This insight underscores the importance of accounting for steric effects in the design and optimization of catalytic systems for enhanced performance.

4.5 Aromaticity

Let's first take a look at the insights of these modifications and how these proposals have the potential to overcome the original structures in the activation of the catalyst. In the following figures, the $\text{Fe}(\text{CO})_3$ moiety is omitted just for clarity.

On the one hand, we introduced a π -conjugated six-membered ring in the tail position of the system. With this, it acquires some extra stability resulting in lower energetic barriers coming from the conjugation of the added ring. For instance, Renaud catalyst's (R) and St.1 complex structure are those which differ from each other concerning this addition (Figure 8).

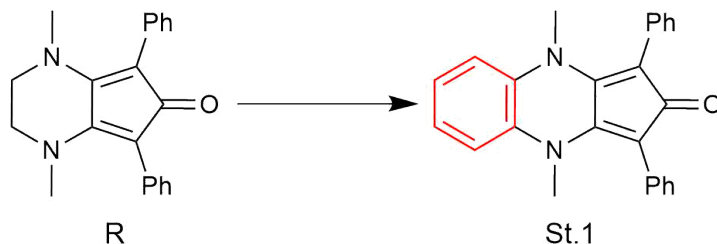


Figure 8: Annulation of the benzene ring to the original Renaud (R) catalyst (marked in red), the $\text{Fe}(\text{CO})_3$ moiety not included for clarity).

As a result of the introduction of the annulated ring, the system is stabilized by around 3 kcal/mol due to the aromatic character of the newly added six-membered ring.

On the other hand, we remove the methyl group coming from the six-membered heteroatomic ring. This causes the formation of two double bonds including a methylenic group and a N atom each one, giving rise to a π -conjugated system occasioning the delocalization of the electron density, therefore providing extra stability to the structure. A representative case is a comparison between Renaud (R) and modified Renaud (St.7) complexes (Figure 9).

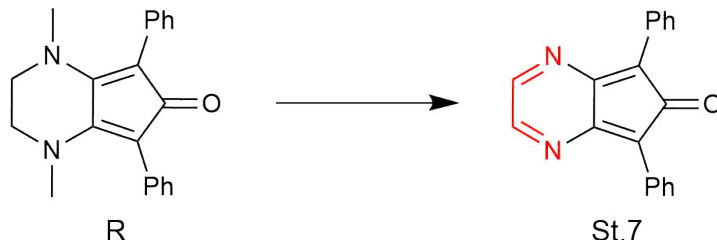


Figure 9: Removal of methyl groups attached to nitrogens and formation of conjugated double bonds (marked in red), the $\text{Fe}(\text{CO})_3$ moiety not included for clarity).

The barrier for the reaction step **I** \rightarrow **II** decreases by 10 kcal/mol due to this modification. As a consequence of it, the two-bonded conjugated system is formed. Since this modification affects the electronic delocalization within the complex, aromaticity will help us understand why this barrier decreases when the methyl groups are removed (Table 6).

Table 6: The aromaticity indexes for Renaud (R) complex and St.7 catalyst for the intermediate **I**.

Catalyst	Ring	MCI	I_{ring}	I_{NG}	I_{NB}	FLU	BOA	BLA	PDI	HOMA
R	1	0,0062	0,0076	0,0310	0,0290	0,0770	0,0176	0,0122	–	-1,2788
	2	0,0004	0,0004	0,0184	0,0171	0,0488	0,0893	0,0367	0,0119	-0,6781
St.7	1	0,0059	0,0071	0,0306	0,0287	0,0752	0,0524	0,0156	–	-1,4825
	2	0,0208	0,0159	0,0344	0,0334	0,0374	0,1774	0,0297	0,0642	0,5772

Examining the MCI, it is clear that the aromaticity of the six-membered ring increases by two orders of magnitude in the case of the Renaud catalyst. This raise in aromaticity is likely facilitated by the lone pair of electrons present in the nitrogen.

This effect is observed not only in the relationship between the original catalyst and its modified form but also after the addition of the conjugated aromatic ring. This can be seen when comparing St.1 with St.2, as well as the catalysts St.3 and St.4 (Figure 10).

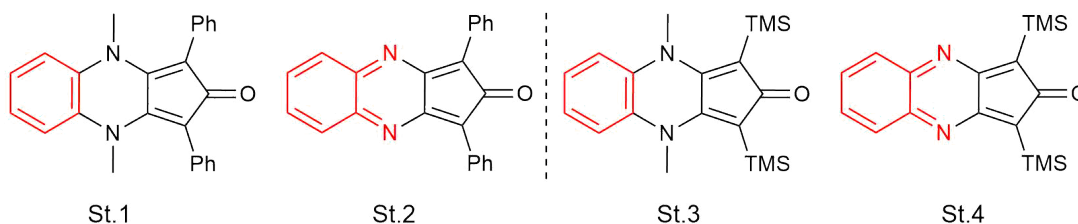


Figure 10: Modifications made (marked in red) compared with the original Renaud structure, the $\text{Fe}(\text{CO})_3$ moiety not included for clarity).

By comparing the calculated activation energies presented in Table 1, we observe a significant reduction of approximately 5 to 10 kcal/mol. This decrease is attributed to the removal of the methyl group, which alters the electronic structure and stabilizes the transition state, thereby lowering the energy barrier for the reaction. When modifying it, it is important to understand the role that electronic delocalization plays in this variation of the energy barrier. This involves analyzing how the distribution of electron density within the complex influences the stabilization of the system, ultimately affecting the overall activation energy required for the reaction (Table 7).

Table 7: The aromaticity indexes for complexes St.1 to St.4 for the intermediate **I**.

Catalyst	Ring	MCI	I_{ring}	I_{NG}	I_{NB}	FLU	BOA	BLA	PDI	HOMA
St.1	1	0,0066	0,0083	0,0315	0,0294	0,0732	0,0055	0,0097	–	-1,1220
	2	0,0024	0,0020	0,0244	0,0233	0,0272	0,0953	0,0263	0,0164	0,4440
	3	0,0524	0,0358	0,0394	0,0390	0,0036	0,0477	0,0100	0,0864	0,8477
St.2	1	0,0054	0,0065	0,0300	0,0282	0,0794	0,0050	0,0038	–	-1,1220
	2	0,0165	0,0124	0,0330	0,0321	0,0256	0,0477	0,0046	0,0594	0,4440
	3	0,0208	0,0166	0,0346	0,0334	0,0258	0,1991	0,0250	0,0568	0,8477
St.3	1	0,0069	0,0090	0,0321	0,0296	0,0558	0,0097	0,0086	–	-1,1802
	2	0,0024	0,0020	0,0243	0,0233	0,0285	0,0890	0,0253	0,0169	0,4325
	3	0,0523	0,0358	0,0393	0,0390	0,0036	0,0481	0,0097	0,0864	0,8534
St.4	1	0,0056	0,0072	0,0307	0,0284	0,0638	0,0205	0,0008	–	-1,5009
	2	0,0166	0,0125	0,0330	0,0322	0,0272	0,0551	0,0046	0,0595	0,2862
	3	0,0207	0,0165	0,0346	0,0334	0,0261	0,2006	0,0243	0,0567	0,3614

Examining the MCI in the first pair of systems reveals a clear aromatic compensation towards the third aromatic ring compared to the other two. As previously mentioned, the presence of methyl groups on the nitrogens prevents the annulated six-membered ring from conjugating with the intermediate ring and, to a greater extent, with the cyclopentadienone. Conversely, in St.2, the aromaticity of this conjugated π -system is partially transferred to the heteroatomic ring. The PDI also supports this explanation, showing that the conjugated system results in a more evenly distributed aromaticity among the rings, thereby stabilizing the system and consequently reducing the barrier.

For the second pair, a similar phenomenon occurs. The most aromatic character is mainly provided by the benzenoid ring, while the others do not contribute to this fact for the first catalyst. However, in St.4, the absence of methyl groups allows the formation of a conjugated system, enabling the external rings to share their aromaticity with the central ring. The PDI similarly demonstrates this change in electron delocalization towards the inner ring upon removal of the methyl groups.

Another of the previously mentioned modifications is observing the effect of adding a substituent to the phenyl group attached to the cyclopentadienone. This modification was studied for the Renaud catalyst [7], concluding that adding an electron-withdrawing group in the *meta* position of the phenyl, especially the trifluoromethyl group (CF_3), causes stabilization of the activation

barrier of the compound. It was noted that this purely electronic effect did not completely affect the catalytic activity due to the distance from the metal center, but still lowered the activation energy. Because of this extra stabilization provided by adding a substituent to the phenyl, it was decided to study this effect in the proposed catalysts (Figure 11).

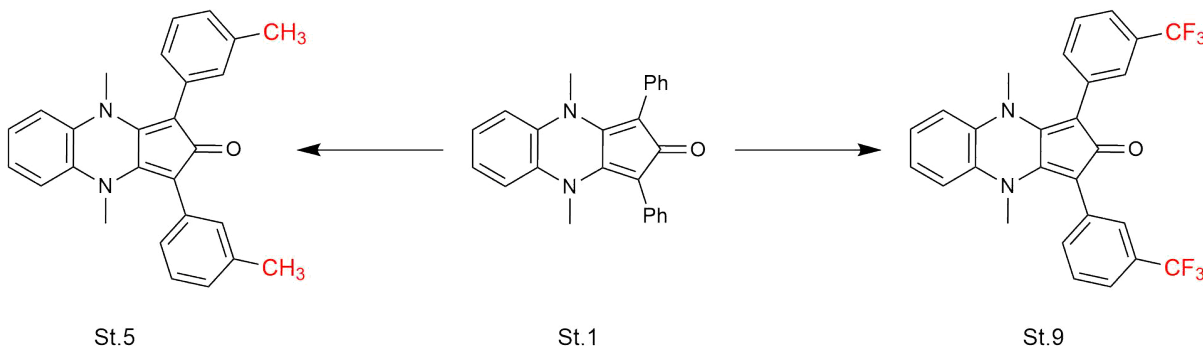


Figure 11: Addition of electron-donating (CH_3) or electron-withdrawing (CF_3) groups at the meta position of phenyls attached to cyclopentadienone (marked in red), the $\text{Fe}(\text{CO})_3$ moiety not included for clarity).

Table 8: The aromaticity indexes for complexes St.1, St.9 and St.5 for the intermediate I.

Catalyst	Ring	MCI	I_{ring}	I_{NG}	I_{NB}	FLU	BOA	BLA	PDI	HOMA
St.1	1	0,0066	0,0083	0,0315	0,0294	0,0732	0,0055	0,0097	–	-1,1220
	2	0,0024	0,0020	0,0244	0,0233	0,0272	0,0953	0,0263	0,0164	0,4440
	3	0,0524	0,0358	0,0394	0,0390	0,0036	0,0477	0,0100	0,0864	0,8477
St.9	1	0,0066	0,0082	0,0315	0,0293	0,0735	0,0599	0,0076	–	-1,1087
	2	0,0024	0,0020	0,0244	0,0234	0,0272	0,1003	0,0282	0,0165	0,4419
	3	0,0526	0,0360	0,0394	0,0390	0,0036	0,0465	0,0098	0,0867	0,8504
St.5	1	0,0066	0,0083	0,0315	0,0293	0,0741	0,0093	0,0089	–	-1,0785
	2	0,0024	0,0021	0,0245	0,0234	0,0264	0,0923	0,0275	0,0138	0,4380
	3	0,0521	0,0357	0,0393	0,0389	0,0036	0,0460	0,0098	0,0860	0,8413

As shown in Table 8, the addition of an electron-withdrawing group (EWG) or an electron-donating group (EDG) does not affect the aromaticity or the structure of the rings or the cyclopentadienone itself. The difference in activation energy between catalysts St.5 and St.9, as previously discussed, may be attributed to the overall stabilization provided by the CF_3 group compared to the methyl substitution on the phenyl rings.

Previous modifications have demonstrated that the addition of a six-membered aromatic ring facilitates reactions within the catalytic cycle by lowering activation barriers due to the additional stability it provides. Taking this into consideration, the final modification to explore is the incorporation of substituents on the mentioned aromatic ring. Previous modifications have indicated that electron acceptor groups contribute additional stability to the system, enhancing its overall performance. Therefore, the proposed modification will involve introducing CF_3 groups at the terminal positions of the main structure (Figure 12), as these groups are known for their electron-withdrawing properties, which can further influence the electronic characteristics and stability of the catalytic system.

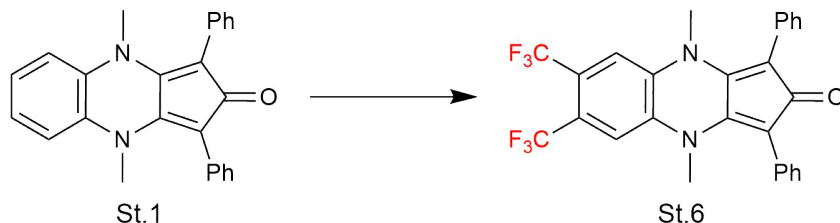


Figure 12: Addition of electron-withdrawing groups (CF_3) to the annulated six-membered ring (marked in red), the $\text{Fe}(\text{CO})_3$ moiety not included for clarity).

Applying this final modification results in a decrease in the activation energy values. This decrease, although not substantial, ranges approximately between 0.5 and 1.9 kcal/mol. To understand the impact of adding these groups, and as it involves a modification affecting the electronic structure, we can refer to various aromaticity indices (Table 9).

Table 9: The aromaticity indexes for complexes St.1 and St.6 for the intermediate **I**.

Catalyst	Ring	MCI	I_{ring}	I_{NG}	I_{NB}	FLU	BOA	BLA	PDI	HOMA
St.1	1	0,0066	0,0083	0,0315	0,0294	0,0732	0,0055	0,0097	–	-1,1220
	2	0,0024	0,0020	0,0244	0,0233	0,0272	0,0953	0,0263	0,0164	0,4440
	3	0,0524	0,0358	0,0394	0,0390	0,0036	0,0477	0,0100	0,0864	0,8477
St.6	1	0,0066	0,0083	0,0315	0,0293	0,0749	0,0121	0,0099	–	-1,1371
	2	0,0026	0,0022	0,0248	0,0236	0,0255	0,0588	0,0186	0,0137	0,4855
	3	0,0444	0,0310	0,0384	0,0379	0,0050	0,0332	0,0077	0,0766	0,8312

The MCI values for the fused ring show a slight decrease because of the CF_3 group withdraws electron density from the conjugated ring, causing it to lose some of its aromatic character. Additionally, the PDI, which indicates electron delocalization among positions in six-membered rings, also shows a decrease in the calculated value for the terminal ring, indicating a reduction in aromatic character.

However, linking the increase in reactivity with stabilization by aromaticity of intermediate **I** is risky, and what is presented here is a starting point for future calculations. If intermediates are stabilized, the barriers rise. It would be nice to do the analysis in the transition state, or even better, to see if there is a significant change in aromaticity going from the intermediate to the transition state that might explain the different barriers. Then, focus on the barrier **III** \rightarrow **IV** which is part of the catalytic cycle, since **I** \rightarrow **II** is a reaction that prepares the catalyst but this reaction is only important at the beginning, therefore it is a choice but that once overcome does not slow down the reaction. Once you have a large enough concentration of active catalyst, the important reaction is **III** \rightarrow **IV**. Therefore, it is necessary to consider whether aromaticity plays a key role in the **III** \rightarrow **IV** barrier and whether the conclusions drawn with precatalyst **I** can be extrapolated (see tables in Appendix A.2).

5 Conclusions

This work has explored the potential of modified Knölker-type iron complexes as catalysts for catalytic hydrogenation, emphasizing their sustainability and efficiency compared to traditional noble metal catalysts. By investigating the structural modifications on the cyclopentadienone framework, the research aimed to understand how these changes impact the catalytic cycle.

The computational analyses revealed that altering the substituents on the cyclopentadienone structure significantly reduces the energy barriers, enhancing both reactivity and chemoselectivity. These modifications not only improve the efficiency of the hydrogenation process but also influence the conditions under which the synthesis of these complexes can occur. The use of advanced computational techniques provided a detailed understanding of the electronic and geometric properties of the catalysts, offering valuable insights into their reactivity and interaction patterns.

The findings of this research contribute to the field of predictive catalysis, demonstrating that careful structural modifications can lead to the development of more efficient and sustainable catalysts. This work underscores the importance of leveraging computational methods to accelerate the discovery and optimization of new catalytic systems, aligning with the broader goals of sustainable and environmentally friendly chemical processes.

In conclusion, this thesis highlights the potential of first-row transition metals, particularly iron, as viable alternatives to noble metals in catalytic hydrogenation. The success of the modified Knölker-type iron complexes paves the way for further advancements in catalyst design, promoting more sustainable practices in the chemical and pharmaceutical industries. Future research should continue to explore and refine these modifications, aiming to fully realize the benefits of sustainable catalysis.

References

- [1] F. D. Klingler. “Asymmetric Hydrogenation of Prochiral Amino Ketones to Amino Alcohols for Pharmaceutical Use”. In: *Accounts of Chemical Research* 40 (2007), pp. 1367–1376.
- [2] Q. Zhou and J. Xie. “ChemInform Abstract: Transition Metal-Catalyzed Enantioselective Hydrogenation of Enamides and Enamines”. In: *ChemInform* 46 (2015), chin.201547245.
- [3] T. Ikariya, K. Murata, and R. Noyori. “Bifunctional transition metal-based molecular catalysts for asymmetric syntheses”. In: *Organic Biomolecular Chemistry* 4 (2006), pp. 393–406.
- [4] Y. Shvo et al. “A new group of ruthenium complexes: structure and catalysis”. In: *Journal of the American Chemical Society* 108 (1986), pp. 7400–7402.
- [5] C. P. Casey and H. Guan. “Cyclopentadienone Iron Alcohol Complexes: Synthesis, Reactivity, and Implications for the Mechanism of Iron-Catalyzed Hydrogenation of Aldehydes”. In: *Journal of the American Chemical Society* 131 (2009), pp. 2499–2507.
- [6] H.-J. Knölker et al. “Demetalation of Tricarbonyl(cyclopentadienone)iron Complexes Initiated by a Ligand Exchange Reaction with NaOH—X-Ray Analysis of a Complex with Nearly Square-Planar Coordinated Sodium”. In: *Angewandte Chemie International Edition* 38 (1999), pp. 2064–2066.
- [7] N. Joly et al. “Enhancement of Knölker Iron Catalysts for Imine Hydrogenation by Predictive Catalysis: From Calculations to Selective Experiments”. In: *Organometallics* 42 (2023), pp. 1784–1792.
- [8] C. Huo et al. “Catalyzed Chemoselective Acrolein Hydrogenation. Density Functional Studies”. In: *Organometallics* 23 (2004), pp. 2168–2178.
- [9] M. J. Frisch et al. *Gaussian 09 Revision E.01*. Gaussian Inc. Wallingford CT 2009.
- [10] A. D. Becke. “Density-functional exchange-energy approximation with correct asymptotic behavior”. In: 38 (1988).
- [11] A. Schäfer, H. Horn, and R. Ahlrichs. “Fully optimized contracted Gaussian basis sets for atoms Li to Kr”. In: 97 (1992).
- [12] W. Küchle et al. “Energy-adjusted pseudopotentials for the actinides. Parameter sets and test calculations for thorium and thorium monoxide”. In: 100 (1994).
- [13] *Chemcraft - Graphical program for visualization of quantum chemistry computations*.
- [14] J. P. Perdew. “Density-functional approximation for the correlation energy of the inhomogeneous electron gas”. In: 33 (1986).
- [15] F. Weigend and R. Ahlrichs. “Balanced basis sets of split valence, triple zeta valence and quadruple zeta valence quality for H to Rn: Design and assessment of accuracy”. In: 7 (2005).
- [16] V. Barone and M. Cossi. “Quantum Calculation of Molecular Energies and Energy Gradients in Solution by a Conductor Solvent Model”. In: 102 (1998).
- [17] I. Mayer. “Charge, bond order and valence in the AB initio SCF theory”. In: *Chemical Physics Letters* 97 (1983), pp. 270–274.

- [18] S. I. Gorelsky. “Quantitative descriptors of electronic structure in the framework of molecular orbital theory”. In: *Advances in Inorganic Chemistry*. Vol. 73. Elsevier, 2019, pp. 191–219.
- [19] W. Yang and W. J. Mortier. “The use of global and local molecular parameters for the analysis of the gas-phase basicity of amines”. In: *Journal of the American Chemical Society* 108 (1986), pp. 5708–5711.
- [20] L. Falivene et al. “Towards the online computer-aided design of catalytic pockets”. In: *Nature Chemistry* 11 (2016), pp. 872–879.
- [21] A. Poater et al. “Samb V ca: A Web Application for the Calculation of the Buried Volume of N-Heterocyclic Carbene Ligands”. In: *European Journal of Inorganic Chemistry* 2009 (2009), pp. 1759–1766.
- [22] M. Solà. “Why Aromaticity Is a Suspicious Concept? Why?” In: *Frontiers in Chemistry* 5 (2017).
- [23] I. Casademont Reig. “Computational study of Aromaticity in Porphyrinoid Systems and Photosensitizers from Chemical Bonding Descriptors”. Theoretical Chemistry and Computational Modeling. Donostia: Universidad del País Vasco/Euskal Herriko Unibertsitatea, 2021.
- [24] E. Matito. *New tools for chemical bonding analysis notes*.
- [25] J. Kruszewski and T.M. Krygowski. “Definition of aromaticity basing on the harmonic oscillator model”. In: *Tetrahedron Letters* 13 (1972), pp. 3839–3842.
- [26] M. Giambiagi et al. “Multicenter bond indices as a measure of aromaticity”. In: *Physical Chemistry Chemical Physics* 2 (2000), pp. 3381–3392.
- [27] F. Feixas et al. “Aromaticity of Distorted Benzene Rings: Exploring the Validity of Different Indicators of Aromaticity”. In: *The Journal of Physical Chemistry A* 111 (2007), pp. 4513–4521.
- [28] P. Bultinck, R. Ponc, and S. Van Damme. “Multicenter bond indices as a new measure of aromaticity in polycyclic aromatic hydrocarbons”. In: *Journal of Physical Organic Chemistry* 18 (2005), pp. 706–718.
- [29] E. Matito, M. Duran, and M. Solà. “The aromatic fluctuation index (FLU): A new aromaticity index based on electron delocalization”. In: *The Journal of Chemical Physics* 122 (2005), p. 014109.
- [30] R. L. Fulton. “Sharing of electrons in molecules”. In: *The Journal of Physical Chemistry* 97 (1993), pp. 7516–7529.
- [31] R. F. W. Bader et al. “Electron Delocalization and the Fermi Hole”. In: *Journal of the American Chemical Society* 118 (1996), pp. 4959–4965.
- [32] J. Poater et al. “The Delocalization Index as an Electronic Aromaticity Criterion: Application to a Series of Planar Polycyclic Aromatic Hydrocarbons”. In: *Chemistry – A European Journal* 9 (2003), pp. 400–406.
- [33] N. Li and W. Zhang. “Frustrated Lewis Pairs: Discovery and Overviews in Catalysis”. In: *Chinese Journal of Chemistry* 38 (2020), pp. 1360–1370.

-
- [34] P.P. Zamora et al. “Theoretical determination of a reaction intermediate: Fukui function analysis, dual reactivity descriptor and activation energy”. In: *Journal of Molecular Structure* 1227 (2021), p. 129369.
- [35] E. Matito. *ESI-3D Electron Sharing Indexes Program for 3D Molecular Space Partitioning*. Girona, 2006.

A Appendix

A.1 Steric maps for intermediate III

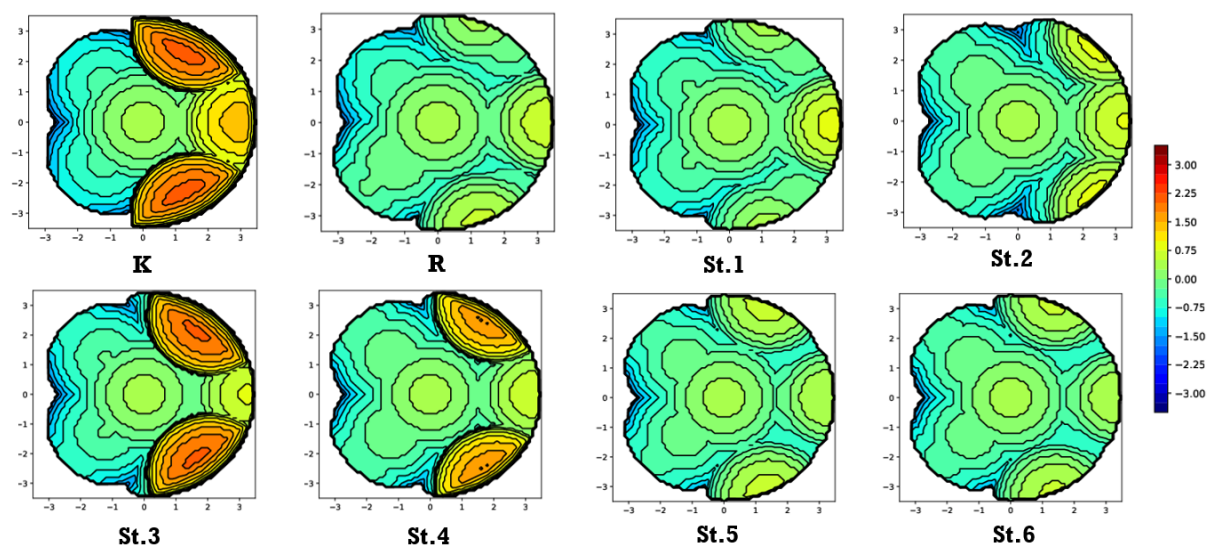


Figure A1: Steric maps (plane xy) of the intermediate **III** for the studied iron complexes, with a radius of 3.5 Å. The metal center of the catalysts are at the origin. The isocontour curves of the steric maps are given in Å.

A.2 Tables of aromaticity indices for the others intermediates

Table A1: The aromaticity indexes for Renaud complex for the intermediate **III**.

Catalyst	Ring	MCI	I_{ring}	I_{NG}	I_{NB}	FLU	BOA	BLA	PDI	HOMA
R	1	0,0063	0,0078	0,0312	0,0290	0,0747	0,0057	0,0087	–	-1,1732
	2	0,0004	0,0004	0,0184	0,0169	0,0492	0,0859	0,0354	0,0119	-0,6889

Table A2: The aromaticity indexes for Knölker complex for the intermediate **III**.

Catalyst	Ring	MCI	I_{ring}	I_{NG}	I_{NB}	FLU	BOA	BLA	PDI	HOMA
K	1	0,0086	0,0108	0,0332	0,0309	0,0473	0,0749	0,0125	–	-0,9886
	2	0,0005	0,0005	0,0195	0,0180	0,0819	0,0360	0,0092	0,0127	-3,8154

Table A3: The aromaticity indexes for complex St.1 for the intermediate **III**.

Catalyst	Ring	MCI	I_{ring}	I_{NG}	I_{NB}	FLU	BOA	BLA	PDI	HOMA
St.1	1	0,0069	0,0086	0,0318	0,0296	0,0707	0,0009	0,0085	–	-1,0321
	2	0,0024	0,0020	0,0243	0,0232	0,0280	0,0929	0,0250	0,0159	0,4402
	3	0,0521	0,0357	0,0393	0,0389	0,0037	0,0464	0,0097	0,0861	0,8451

Table A4: The aromaticity indexes for complex St.2 for the intermediate **III**.

Catalyst	Ring	MCI	I_{ring}	I_{NG}	I_{NB}	FLU	BOA	BLA	PDI	HOMA
St.2	1	0,0057	0,0068	0,0304	0,0285	0,0767	0,0102	0,0024	–	-1,4973
	2	0,0157	0,0119	0,0328	0,0319	0,0270	0,0618	0,0083	0,0588	0,3308
	3	0,0199	0,0160	0,0344	0,0332	0,0270	0,2054	0,0259	0,0559	0,3667

Table A5: The aromaticity indexes for complex St.3 for the intermediate **III**.

Catalyst	Ring	MCI	I_{ring}	I_{NG}	I_{NB}	FLU	BOA	BLA	PDI	HOMA
St.3	1	0,0072	0,0093	0,0323	0,0298	0,0539	0,0149	0,0078	–	-1,0757
	2	0,0024	0,0020	0,0243	0,0233	0,0291	0,0860	0,0241	0,0161	0,4369
	3	0,0519	0,0355	0,0393	0,0389	0,0037	0,0477	0,0096	0,0859	0,8500

Table A6: The aromaticity indexes for complex St.4 for the intermediate **III**.

Catalyst	Ring	MCI	I_{ring}	I_{NG}	I_{NB}	FLU	BOA	BLA	PDI	HOMA
St.4	1	0,0060	0,0077	0,0311	0,0288	0,0614	0,0265	0,0011	–	-1,3786
	2	0,0159	0,0120	0,0328	0,0319	0,0287	0,0661	0,0073	0,0590	0,2523
	3	0,0199	0,0160	0,0344	0,0332	0,0271	0,2058	0,0250	0,0559	0,3321

Table A7: The aromaticity indexes for complex St.5 for the intermediate **III**.

Catalyst	Ring	MCI	I_{ring}	I_{NG}	I_{NB}	FLU	BOA	BLA	PDI	HOMA
St.5	1	0,0068	0,0085	0,0317	0,0295	0,0720	0,0038	0,0083	–	-1,0014
	2	0,0024	0,0020	0,0244	0,0233	0,0272	0,0890	0,0258	0,0135	0,4446
	3	0,0517	0,0355	0,0393	0,0389	0,0037	0,0422	0,0092	0,0857	0,8382

Table A8: The aromaticity indexes for complex St.6 for the intermediate **III**.

Catalyst	Ring	MCI	I_{ring}	I_{NG}	I_{NB}	FLU	BOA	BLA	PDI	HOMA
St.6	1	0,0069	0,0086	0,0318	0,0296	0,0723	0,0037	0,0084	–	-1,0496
	2	0,0025	0,0022	0,0247	0,0235	0,0264	0,0571	0,0175	0,0135	0,4860
	3	0,0440	0,0307	0,0384	0,0378	0,0051	0,0292	0,0068	0,0762	0,8287

Table A9: The aromaticity indexes for complex St.7 for the intermediates **I** and **III**.

Catalyst	Ring	MCI	I_{ring}	I_{NG}	I_{NB}	FLU	BOA	BLA	PDI	HOMA
St.7 - I	1	0,0059	0,0071	0,0306	0,0287	0,0752	0,0524	0,0156	–	-1,4825
	2	0,0208	0,0159	0,0344	0,0334	0,0374	0,1774	0,0297	0,0642	0,5772
St.7 - III	1	0,0062	0,0075	0,0309	0,0290	0,0727	0,0605	0,0177	–	-1,3827
	2	0,0194	0,0149	0,0340	0,0330	0,0402	0,1897	0,0329	0,0624	0,5444

Table A10: The aromaticity indexes for complex St.8 for the intermediates **I** and **III**.

Catalyst	Ring	MCI	I_{ring}	I_{NG}	I_{NB}	FLU	BOA	BLA	PDI	HOMA
St.8 - I	1	0,0081	0,0096	0,0325	0,0305	0,0646	0,0308	0,0127	–	-1,1364
	2	0,0005	0,0005	0,0196	0,0181	0,0809	0,0427	0,0097	0,0128	-3,7739
St.8 - III	1	0,0084	0,0100	0,0328	0,0308	0,0623	0,0486	0,0106	–	-1,0420
	2	0,0005	0,0005	0,0196	0,0181	0,0816	0,0389	0,0100	0,0128	-3,7735

Table A11: The aromaticity indexes for complex St.9 for the intermediate **III**.

Catalyst	Ring	MCI	I_{ring}	I_{NG}	I_{NB}	FLU	BOA	BLA	PDI	HOMA
St.9	1	0,0068	0,0085	0,0317	0,0295	0,0710	0,0650	0,0082		-1,0211
	2	0,0024	0,0020	0,0243	0,0233	0,0280	0,0982	0,0271	0,0159	0,4387
	3	0,0523	0,0358	0,0394	0,0390	0,0036	0,0450	0,0095	0,0864	0,8487

Table A12: The aromaticity indexes for complex St.10 for the intermediates **I** and **III**.

Catalyst	Ring	MCI	I_{ring}	I_{NG}	I_{NB}	FLU	BOA	BLA	PDI	HOMA
St.10 - I	1	0,0066	0,0083	0,0315	0,0294	0,0732	0,0055	0,0097	–	-1,1220
	2	0,0024	0,0020	0,0244	0,0233	0,0272	0,0953	0,0263	0,0164	0,4440
	3	0,0524	0,0358	0,0394	0,0390	0,0036	0,0477	0,0100	0,0864	0,8477
St.10 - III	1	0,0066	0,0083	0,0315	0,0293	0,0749	0,0121	0,0099	–	-1,1371
	2	0,0026	0,0022	0,0248	0,0236	0,0255	0,0588	0,0186	0,0137	0,4855
	3	0,0444	0,0310	0,0384	0,0379	0,0050	0,0332	0,0077	0,0766	0,8312